Experimental study on yielding and relief pressure support technology of fluid-filled lining in a high-ground stress soft rock tunnel

Jie Liu[1,2], Bin Wang[1,2], Yunan Yang[1,2*],Haoyu Yang[1,2],Yansong Wang[1,2], Zhuoxing Du[1,2]

[1] College of Civil Engineering & Architecture, China Three Gorges University, Yichang City, Hubei Province,443002, China
[2] Key Laboratory of Geological Hazards on Three Gorges Reservoir Area, Ministry of Education, China Three Gorges University, Yichang City, Hubei Province, 443002, China

*Corresponding author: Yunan Yang, e-mail: yangyunan_11@126.com

Abstract

High-ground stress soft rock tunnels have experienced large deformations. Yielding and pressure relief fluid-filled lining support technology is an effective method for solving large soft rock tunnel deformation due to the deformation characteristics of high-ground stress soft rock tunnels. To give the surrounding rock a certain amount of deformation space, a layer of fluid filling is set up at the reserved deformation of the tunnel. By creating a force test model of the inflatable carcass and water-filled carcass, the straight section of the tunnel support structure is simulated. When supporting large deformation soft rock tunnels, inflatable and water-filled carcasses produce fluid homogenization load shedding and fluid drainage load shedding effects. Inflatable carcasses and water-filled carcasses without leakage reduce load by about 28% and 7%, respectively. The peak load reduction rate under liquid leakage can gradually reach 100 %. Inflatable carcasses can dissipate up to 90% of the work of external forces acting on the supporting structure. The load reduction rate of water-filled carcass is 1.2 times that of inflatable carcass. Fluid-filled materials can remove load from secondary lining support structures after yielding and pressure relief. Design and construction of high-ground stress soft rock tunnels can be influenced by research results.

Keywords

Fluid-filled lining, large deformation, high-ground stress, soft rock tunnel, yielding pressure, relief pressure

1 Introduction

A rapidly developing world economy is allowing engineering constructions to gradually open up to deep rock masses trapped in complicated deep geological structures. Due to the recent construction of strategic infrastructure in the western complex and difficult mountainous areas, tunnel projects have emerged as "long, large, deep and difficult" [1]. When extensive soft rock excavation occurs, the rock mass will exhibit giant creep, prolonged deformation time, and high deformation rate [2]. With more and more deep buried tunnels and more complex geological conditions, the problem of large deformation in high stress soft rock tunnels is becoming more and more serious[3], and it seriously restricts the construction safety and long-term operational stability of the tunnel project[4]. For example, the deformation of the surrounding rock of the Wushaoling Tunnel is as high as 105.3cm, which caused severe damage to the initial support of the tunnel and has intruded into the supporting structure of the second lining [5]; The arch settlement of Muzhailing Tunnel of Lanzhou-Chongqing Railway is 1712mm, the maximum convergence of Jiazhujing Tunnel of Nanzhou-Kunming Railway is 1600mm, and the arch settlement of Wuzhaoling Tunnel of Lanzhou-Xinjiang Railway is 1209mm [6]. Tunnel engineering development therefore requires a supporting technology that resists soft rock tunnel deformation, is safe and low-cost.

The safety and stability of a deep tunnel after excavation depend primarily on the influence of the rheology of the surrounding rock of the tunnel on the bearing performance of the supporting structure [7]. To analyze tunnel support, research on reasonable excavation layouts and different supports has gradually become a crucial factor that must be considered [8]. Still, before solving the support problem, it is necessary to clarify the deformation and failure mechanism. This includes factors and laws of deep soft rock roadways, etc. [9] and then propose effective support methods in targetedly. To improve the safety and stability of tunnel support work, the overall rigidity of the tunnel support structure is increased. For example, the "double-layer long bolt and shotcrete steel pipe concrete" combined support scheme is used in the deep soft rock roadway in the second mining area of Jinchuan Mine in Gansu Province [9]. Because of the severe subsidence of the roadway floor and obvious bottom heave caused by the return air roadway of the Xinhu Coal Mine in Haozhou,

the full-face double-layer arch synergistic reinforcement technology is used to propose the “shotcrete + grouting bolt + anchor rod + grouting anchor cable + anchor cable” composite support method [10] and a method of applying sufficient prestress to the supporting structure mainly consisting of anchor cables, anchor rods, and shot crete, etc [11]. Although soft rock tunnel support technology is increasingly popular, it has not been applied to smooth rock tunnel support technology.The reason is that mild, severe rock roadway conditions are complex. It isn't easy to find the most efficient way for tunnels with different surrounding rock characteristics and reasonable and identical support methods [12].

Tunnel support structures interact with surrounding rock and deform together. Part of the energy is released by the surrounding rock and absorbed by the support structure. However, the total energy remains unchanged. Tunnels tend to undergo relatively large static and dynamic deformations under high stress. It is impossible to control the energy involved through more robust supports. Conventional rigid support methods cannot resist large soft rock deformations at high rates. Tunnels supported by conventional support systems face a significant challenge due to the large convergence at the tunnel boundary [13-15]. When the host rock fails, significant plastic deformations could occur. On the contrary, the supporting structure must have a pressure-reducing function to effectively absorb the deformation energy of the surrounding rock [16]. Scholars began to consider modifying various supporting structures to reduce pressure. In tunnel support technology, bolt support technology has unique advantages. To compensate for flexible pressure relief, a constant resistance squeeze slip pressure relief bolt is proposed to absorb the energy of rock deformation caused by high ground stress [17] and a new type of bolt-deformation control bolt is also available (DC-bolt) [18]. A novel prestressed yield bolt with the engineering background of Shangping roadway in Huafeng Coal Mine is proposed [19]. A new constant resistance and yielding support technology based on a large deformation anchor cable is proposed to control large deformations of surrounding rocks [20]. In addition to anchor rods, steel arches are also a significant part of the tunnel support structure. Therefore, the U-shaped steel and anchor net combined support scheme with pressure relief effect was proposed for use in large deformation tunnels [21]. Yu et al [22] propose a short bolt, long anchor cable, and U-shaped steel bracket combined support program. In addition, a new type of high deformation concrete with a yield support system achieves pressure relief support through concrete deformation and has applied the support system in a deep tunnel [23].

Since the pressure relief effect of the supporting structure has certain limitations, it is proposed to set a buffer layer between the secondary lining and the surrounding rock that can absorb the rheological deformation of the surrounding rock [24]. Y. Tian el at [25] suggest useing yielding layers to address the squeezing deformation of tunnels. a laboratory test is conducted to verify the effect of the yielding support. The test results show that the pressure of the secondary lining is reduced with the installation of the yielding layer. Tian el at [26] proposes a radial yielding support with a compressible layer as a solution for large deformation. Based on the proposed design method of yielding support, PE-foam with a density of 90 kg/m^3-100 kg/m^3 is used as the filling material in the compressible layer. The PE-foam compressible layer is used to prevent the damage of the secondary lining of the squeezed tunnel. The buffer layer material has ideal elastoplastic properties and is unique. The mechanical properties enable it to coordinate with the surrounding rock deformation. By absorbing long-term deformation energy, it stabilizes the weak tunnel surrounding stone over time. Considering the soft rock strength weakening buffer layer pressure support of design research [27] as a kind of buffer layer material, foam concrete has the characteristics of high deformability and low density. The use of foamed concrete in tunnel support can absorb a certain amount of rock creep deformation, reduce the lining pressure and provide an excellent solution to the significant deformation problem of squeezed tunnels [28], and Wu et al [29] propose that the use of yielding supports is an extremely effective measure for tunneling in squeezing grounds because of their agreement with the law of mechanical movement of rock mass. The circumferential yielding support sets up the yielding device in the circumferential direction of the tunnel to realize the rigid-flexible-rigid characteristics of the supporting structure [30,31]. Highly deformable elements for a tunnel excavated in squeezing rock is used for design of the yielding support, and the support characteristic of the lining using highly deformable elements and the ground pressure considering strain-softening of soft rock are analyzed by an analytical method [32]. The combined support of circumferential yielding and prestressed anchor cable yielding is proposed, and the mechanical perfor-

mance of the support system is better [33]. In order to solve the failure of support structure of tunnel in high stress soft rock, based on the principle of reasonably releasing the stress in surrounding rocks and reducing the stress of support structure, a tunnel graded yielding support structure is proposed [34,35].

When synthesizing existing support techniques and systems, rigid support technology is primarily used for point or line reinforcement, emphasizing solid support and a hard top; however, this is insufficient to support soft rocks that undergo large deformations over time. Existing flexible support technology can only create controllable support forces in point or line form. However, it cannot produce controllable and homogenized surface support within a wide range of free faces. Therefore, yielding pressure and relief pressure support technology of setting a compressible buffer layer with liquid filled material(inflatable and water-filled carcass) at the reserved deformation volume is innovatively proposed. Using the fluidity of the fluid filled material forms a controllable and homogenized surface support force. The compressibility of the fluid filled material absorbs the pressure generated by the deformation of the surrounding rock, which plays a yielding role. Using the automatic discharge of the fluid filled material releases the surrounding rock pressure, which has a better pressure relief effect. The fluid filled lining utilizes its yielding pressure and relief pressure to absorb and evenly transfer the pressure generated by the deformation of the surrounding rock and ensure the safety and stability of the supporting structure.

Therefore, the author takes the large amount of deformation, long deformation time and uneven distribution of surrounding rock stress of soft rock tunnel as the starting point, the fluid filled material (inflatable and water-filled carcass) is set between the primary support and the secondary lining as the buffer layer of soft rock tunnel, and the automatic pressure relief valve is installed. The force test model of the simply supported beam of the fluid-filled is established to simulate the force of the straight section of the tunnel support structure. The fluid homogenization load reduction effect and the fluid discharge load reduction effect of the fluid filled material on the support process of the large deformation soft rock tunnel are analyzed. The energy conversion analysis model is established for the concentrated loading process of the simply supported beam of the fluid-filled material without pressure relief, and the energy dissipation of the fluid filled material on the supporting structure is calculated. Under pressure relief, the unloading rates of different fluid discharges are analyzed. This research has certain reference value for designing and constructing new tunnel support structures, and it provides a new method of supporting soft rock tunnels.

2 The technical principle of pressure relief support for fluid filled lining

2.1 Force mechanism at different support stages

As shown in Fig. 1, the fluid filled lining support can be divided into three stages, and the force mechanisms are as follows:

(1) Initial installation stage of fluid filled lining: After the tunnel is excavated, the primary lining is completed. Second lining support is carried out immediately, and fluid-filled is filled at the reserved deformation amount to form large-scale surface support quickly. The bladder pressure is P_1, the steel arch bearing load is q_1, and the pressure relief threshold P_3 is set and $P_1 < P_3$, which significantly shortens the deformation time of the surrounding rock surface and reduces the development depth of the loose zone.

(2) Homogenisation pressurization stage below the pressure relief threshold: With the sizeable local deformation of the surrounding rock, the pressure in the inclusion increases from P_1 to P_2, and $P_2 < P_3$ during the pressurization process below the pressure relief threshold because the fluid has good fluidity and has the effect of local homogenization and load reduction so that the supporting structure is uniformly stressed and the problem of significant unevenness of the steel arch frame is effectively avoided.

(3) Fluid-filled automatic pressure relief stage: With the continuous deformation of the surrounding rock, the pressure in the inclusion is higher than the pressure relief threshold P_3. The pressure relief valve or suction equipment is used to actively discharge the fluid to efficiently and quickly remove the fluid lining structure. The stress provides space for the surrounding rock to continue to deform. In this process, the steel arch frame load also remains unchanged.

2.2 Load shedding effect

High ground stress soft rock tunnel of fluid filled lining pressure relief of support technology, that is, at the reserved deformation between the surrounding rock of the tunnel and the second lining, a layer of fluid-filled with good fluidity (such as water, air, sand, engineering debris)

buffer layer because the fluid has the characteristics of forced flow and the characteristics of decompression after removal. The fluid filled lining structure can produce liquid homogenization and load reduction effect (λ_1 effect) in the process of supporting high ground stress soft rock tunnels and fluid discharge load shedding effect (λ_2 effect). This paper studies the homogenized load reduction and discharge reduction characteristics of air and water installed in the tunnel lining structure in the form of a closed carcas

2.3 Automatic pressure relief principle of tire-type lining pressure relief support technology

A mechanical pressure relief valve device was independently developed for the purpose of improving fluid discharge and load reduction in fluid filled linings. The pressure relief valve is detailed in the utility model patent (ZL201921205509.4). The device can set the pressure relief threshold P according to the actual engineering situation. When the air pressure in the carcass is lower than the pressure relief threshold, it will not leak. When the carcass pressure is higher than the pressure relief threshold, its internal pressure will decrease as air is discharged from the pressure relief hole. Finally, the stress in the carcass will tend to the state where the pressure relief threshold is balanced.

3 Simulation test design of fluid filled lining

The straight section of the fluid-filled lining tunnel is selected as the research object (Fig. 2a). The straight section of the tunnel is approximated as a simply supported beam (Fig. 2b). It is assumed that the simplysupported beam is an ideal simply supported beam during the test. By establishing a fluid-filled simply supported beam force model (as shown in Fig. 2c), the force of the tunnel support structure is simulated, and the loading effect of the local deformation of the surrounding rock on the support structure is investigated. The model of the experiment is shown in Fig.2d. The fluid-filled materials are inflatable and water-filled carcasses.

Data monitoring implementation：Place the lining carcass with one end connected to the barometer and the other end to the automatic pressure relief valve in channel steel with a total length of 1.2 meters. The inner bottom of the channel steel is affixed to a stress plate. The stress plate of the monitoring point position is shown in Fig. 3 using an I-Motion FEP pressure sensor. The system conducts stress monitoring. Strain gauges are attached to the bottom of the channel steel, and the UT7110Y high-speed static strain gauge is used for strain monitoring. At the same time, a dial indicator is installed at the bottom of the channel steel to observe its vertical displacement.

Loading implementation：A cover plate is placed on the carcass, a hydraulic jack is added to the center of the cover plate, and a pressure sensor is placed above it to observe the pressure value accurately. The hydraulic jack is controlled to load from 0kN to 15kN at loading rates of 0.02kN/s, 0.05kN/s, and 0.1kN/s. When the pressure reaches 15kN, the automatic pressure relief valve is adjusted step by step with 2kPa as an order of magnitude. The pressure threshold until the jack is separated from the upper sensor and the monitoring data is recorded throughout the test.

4 Force and deformation analysis of fluid filled lining

4.1 Force analysis of fluid filled lining

4.1.1 Calculation of the bending moment of fluid filled lining

This pressure distribution diagram (Fig.4) shows an example with a simple supported beam with inflatable carcasses and water-filled carcasses lining with a loading rate of 0.1kN/s. The right side of the pressure distribution diagram is selected for analysis. To facilitate the later calculation, the distribution law is simplified to the following formula (1):

$$y = kx + n \quad (1)$$

Where:

k is the pressure distribution coefficient of the concentrated load on the simple supported beam (unit:N/m),

n is the equilibrium pressure of the pressure distribution of the entire load on the simple supported beam (unit:N).

According to the k and n under different concentrated loads, when the focused load is 1kN, the monitoring pressure from the midpoint x can be obtained. The monitoring pressure is measured by a pressure sensor with a diameter of 2cm because the diameter of the pressure sensor is much smaller than the support; therefore assuming that the surface load of the simple supported beam is evenly distributed within this range, the linear load formula (2) of the monitoring point at the distance x, which is from the midpoint can be obtained:

$$Q(x) = \frac{b}{s} \times m \times (k_1 \times x + n_1) \quad (2)$$

Where:

$Q(x)$ is the line load of the monitoring point from the midpoint x(unit: N/m),

b is the channel steel width(unit: m),
s is the effective area of the pressure sensor and is a fixed value(unit: m^2),
m is the same value as the concentrated load(unit:1),
k_1 is the pressure distribution rate when the concentrated load is 1kN(unit: N/m) ,
n_1 is the equilibrium pressure of the pressure distribution when the concentrated load is 1kN(unit:N).
According to the moment section method for analyzing simple supported beams in structural mechanics, the right section of the tire-type lining supported merely beam selected for force analysis, as shown in Fig. 5.
Calculating the bending moment at x, the balance formula (3) of structural mechanics can be obtained:

$$M(x) = \frac{F}{2} \times (\frac{l}{2} - x) - \frac{1}{2} \times Q(\frac{l}{2}) \times (\frac{l}{2} - x)^2 - \frac{1}{2} \times \frac{1}{3} (Q(x) - Q(\frac{l}{2})) \times (\frac{l}{2} - x)^2 \quad (3)$$

Substituting formula (2) into formula (3) to obtain the formula (4) for calculating the bending moment at the midpoint x of the simple supported beam distance of the tire lining:

$$M(x) = \frac{F}{4}(l - 2x) + \frac{bmk_1}{24s}(3l^2 x - l^3 - 4x^3) + \frac{bmn_1}{8s}(4lx - l^2 - 4x^2) \quad (4)$$

Where l is the length of simple supported beam. When the concentrated load is 3kN, the bending moment at $x=0.5$ on the simple supported beam is $M(0.5)_3 = 0.152kN \cdot m$. Summarise the test data and substitute it into the bending moment formula (4) to calculate all the bending moment values. Draw the bending moment value distribution diagrams at different positions of the tire-type lining simple supported beam under various load levels, as shown in Fig. 6.

4.1.2 Analysis of bending moment distribution formula of fluid filled lining

The bending moment diagrams of simply supported beams with inflatable tire lining, water-filled tire lining and non-tire lining under different concentrated forces are analyzed. The distribution of bending moment on simply supported beams can be expressed by the Gaussian function formula(5):

$$y = y_0 + Ae^{-\frac{(x-x_c)^2}{2w^2}} \quad (5)$$

The bending moment diagrams (Fig. 7) of inflatable carcass simple-supported beam, water-filled carcass simple-supported beam and non-tire simple-supported beam under 13 kN concentrated force are analyzed as an example.
(1) The abscissa in the formula (5) represents the monitoring point position. At the abscissa $x = x_c$, the simple supported beam is $y_0 + A$. The value of x_c changes with the loading position. In the test, the loading position of the simple supported beam is the middle span, then $x_c = 0$.
(2) In the formula (5), A is the absolute difference between the maximum positive bending moment and the maximum negative bending moment of a simple supported beam. This increases with the increase in applied load level.
(3) y_0 is the maximum negative bending moment value on a simple supported beam. Since it is difficult to establish a simple supported beam model in an ideal state in actual tests, a negative bending moment y_0 is generated when the simple supported beam is loaded.
(4) w indirectly corresponds to the length range corresponding to half of the bending moment value broader than the maximum absolute difference between the positive and negative bending moment (i.e. A value) on the simple supported beam.

4.1.3 Load equivalence point of simple supported beam

Ignore the unavoidable errors in the test. It is assumed that the simple supported beam in the test is an ideal simple supported beam. There is no negative bending moment at both ends of the beam when a concentrated force is applied in the middle of the span. The middle span bending moment is the maximum bending moment value. That is, $x_c = 0$, $y_0 = 0$, the distribution formula (6) of the bending moment of the combined inflatable tire lining and the simple supported beam of the unlined carcass is:

$$x = \pm w_0 w_1 \sqrt{\frac{2\ln(A_0 / A_1)}{w_1^2 - w_0^2}} \quad (6)$$

Define the coordinate point x obtained by the above formula as the load equivalent point of the simple supported beam without carcass. Draw the load equivalent points of the simple supported beam under different levels of load into a coordinate diagram, such as shown in Fig. 8.
Define the area between the two load equivalence points under the same load level as the bending moment reduction zone of the simple supported beam of the pneumatic carcass and the simply supported beam with a

water-filled carcass. As shown in Fig. 8, the bending moment reduction zone is roughly the simple supported beam coordinate interval x = (–0.21, 0.18), about 1/3 of the simple supported beam length l. It shows that when the surrounding rock stress is concentrated on a certain point of the lining structure, the inflatable tire lining structure can reduce the surrounding rock stress acting on the lining support structure in a certain range near this point.

4.2 Deflection analysis of fluid filling lining

In this example, the concentrated load is continuously loaded from 0kN to 15kN using an inflatable tire lining, water filled tire lining, and without carcass lining at a loading rate of 0.1kN/s. According to the deflection value of the monitoring point, the corresponding deflection curve comparison diagram is drawn, as shown in Fig. 9.

As shown in Fig.9a and Fig.9b, the deflection in the middle of the simple support beam with carcass is obviously smaller than the deflection of the simple support beam without carcass. The deflection on both sides of the simple support beam with carcass is obviously larger than the deflection of the simple support beam without carcass. This indicates that the fluid filled carcass has an obvious homogenizing effect. The fluid-filling material transforms the local concentrated force acting on the secondary lining support structure into the surface uniform force in a larger area, reducing the damage from surrounding rock to the secondary lining structure, maximizing the strength of the support structure, and improving the structural utilization rate.

The deflection at the midpoint of the inflatable carcass lining simple support beam is smaller than the deflection of the water-filled carcass lining simple support beam, as shown in Fig.9c. As load increases, the trend that the deflection at the midpoint of the inflatable tire lining simple support beam is smaller than that at the midpoint of the water-filled tire lining simple support beam is more obvious. Therefore, the inflatable tire lining has better load reduction effect.

4.3 Force analysis of inflatable tire lining under different loading rates

In order to study the effect of loading rate on the force of the tire lining, the inflatable carcass lining is tested by applying a rate of 0.05kN/s and 0.02kN/s, respectively. Test materials, loading equipment and monitoring equipment remain unchanged during the test. The pressure and strain at each monitoring point are recorded according to the test. The bending moment of a simply supported beam is calculated corresponding equation (4). According to the pressure and bending moment at different points, the corresponding pressure distribution Figures 13 and 14, and bending moment distribution Figures 15 and 16 are plotted.

Analyzing Fig. 5a, Fig. 10, it can be concluded that as the loading rate becomes smaller, the pressure at each point of the inflatable carcass simple support beam gradually decreases. The more homogeneous the force is on the tire lining support structure. It shows that the loading rate affects the homogenization effect of the tire lining. The smaller the loading rate is, the better the pressure of local deformation of surrounding rock can be more uniformly transferred to the supporting structure in the lower position, so the lower the rate of surrounding rock deformation, the better the effect of uniformly transferring the uneven deformation of surrounding rock pressure. Thus, the supporting structure can resolve the problems caused by long-term deformation of high-stress soft rock tunnels. From Fig. 7a, Fig. 11, it can be seen that the bending moment at each point of the inflatable tire simple support beam decreases with the decrease of the loading rate, which indicates that when the surrounding rock stress concentrates on a certain part of the lining structure, if the loading rate of the concentrating stress decreases, the fluid-filled lining support structure can better reduce the surrounding rock stress that acts on the lining support structure within a certain range near this part.

5 Research on fluid mass homogenisation and discharge reduction effect

5.1 Analysis and study of the homogenised load shedding effect (λ1 effect) under the condition that the fluid is not discharged

5.1.1 Comparative analysis of force equalisation effect

Analyzing Fig. 8, compared with simple supported beams without a carcass, the overall “height” of the bending moment diagram under different load levels. The “lower body” is narrower and broader. Now define the characteristic value of bending moment distribution concentration R, which is the ratio of the maximum bending moment in the middle of the span to the value of w, as shown in formula (7):

$$R = \frac{M_{\max}}{w} \quad (7)$$

The R value directly reflects the uniformity of the bending moment distribution on the simple supported beam. The smaller the R value, the more even the bending moment is

distributed on the simple supported beam. It can be seen from Fig. 12 that the R value shows a linear upward trend as the load increases. $R_1 > R_2 > R_3$, which indicates that the pneumatic and water-filled carcass can effectively equalise the force of the lining structure, and it also shows that the pneumatic carcass is homogenised. Force is better than water-filled carcass.

5.1.2 Analysis of partial load reduction effect of pneumatic carcass

It can be seen in Fig. 13 that the mid-span bending moments of different simple supported beams all change linearly with the increase of the load. The mid-span bending moments of simple supported beams with inflated and water-filled carcasses are different from those without reduced carcass. Further, analyse the reduction degree of the half-span bending moment of the pneumatic tire lining simple supported beam relative to the supported merely beam without tire lining under different levels of load and define the half-span bending moment reduction rate as shown in formula (8):

$$r = \frac{M_{0,\max} - M_{1,\max}}{M_{0,\max}} \qquad (8)$$

Where M_{0max} is the maximum mid-span bending moment of the simple supported beam without tire lining and M_{1max} is the maximum mid-span bending moment of the simple supported beam with inflatable tire lining. Substitute the maximum mid-span bending moment data of the carcass-less lining and the inflatable tire-lined simple supported beam under each level of load into the above equation (8) and draw the mid-span bending moment reduction rate analysis diagram (Fig. 14).

Fig. 14 shows that in the non-relief state, the inflatable carcass reduces load significantly better than the water-filled carcass. When the load applied to the inflatable carcass simple supported beam is 2kN in the test, the maximum mid-span bending moment reduction rate of the inflatable carcass simple supported beam is about 28%. When the load is 15kN, the mid-span bending moment reduction rate is reduced to 14% left and right. This indicates that the tire-type lining buffer layer provides larger deformation space and absorbs partial stress from the surrounding rock. Still, as the applied load increases, the internal pressure of the carcass gradually increases. The efficiency of lining load shedding decreases accordingly.

5.1.3 Energy Conversion Analysis

In order to analyse the energy conversion problem of the simple supported beam of the inflated and water-filled carcass during the compression process when the pressure is not relieved, the force model of the simply supported carcass beam shown in Fig. 15 is established.

When the hydraulic jack is directly used to pressurize the carcass on the simple supported beam, the contact area between the jack and the carcass is small. In order to avoid affecting the airtightness of the carcass and the upturning of both sides of the carcass, place lightweight cladding plate on the carcass and bind it with channel steel to reduce adverse effects. It is assumed that the cladding plate will not be bent and deformed during the force process and only produce rigid body displacement. According to the analysis of the law of conservation of energy, it can be seen that the energy of the tire lined simply supported beam structure in the test is shown in Equation (9) :

$$W = W_T + W_C \qquad (9)$$

W is the work done on the concentrated load applied to the simple supported beam, W_T is the energy absorbed by the inflated and water-filled carcass during compression and W_C is the uniformised force of the carcass received by the channel steel work done.

Now take the energy conversion process of a simple supported beam with an inflatable carcass under an external load of 1-10kN as an example for analysis.

It is found from Fig.16 that when the simple supported beam of the inflatable carcass is slowly pressurised with a hydraulic jack, the external force is loaded from 0kN to 10kN and the falling height of the cover plate increases linearly with the change in the external force.

The work done by the concentrated load on the simple supported beam of the inflatable carcass is calculated by the following formula (10):

$$W = \frac{1}{2} F \times \Delta h \qquad (10)$$

Part of the work done by external forces on the simple supported beam of the inflatable carcass is absorbed by the inflatable carcass. The other part is transferred to the channel steel. The energy received by the channel steel is the total work done by the distributed force at the bottom of the channel steel. The specific calculation process is as follows formula (11):

$$W_C = \int_l \frac{b}{2s}(kx + n)\left(y_0 A e^{-\frac{(x-x_C)^2}{2w^2}}\right)dx \qquad (11)$$

$$= \frac{b}{2s}(\int_1 y_0(kx+n)dx + \int_l Akxe^{-\frac{(x-x_c)^2}{2w^2}}dx + \int_1 Ane^{-\frac{(x-x_c)^2}{2w^2}}dx)$$

$$W_C = \int_l \frac{b}{2s}(kx+n)(y_o + Ae^{-\frac{(x-x_c)^2}{2w^2}})dx$$

$$= \frac{b}{2s}(\int_l y_0(kx+n)dx + \int_l Akxe^{-\frac{(x-x_c)^2}{2w^2}}dx + \int_l Ane^{-\frac{(x-x_c)^2}{2w^2}}dx) \quad (11)$$

Organise the above formula (11) leads to formula (12):

$$W_C = \frac{b}{2s}[(y_0kx^2 + 2y_0nx - 2Akw^2e^{-\frac{(x-x_c)^2}{2w^2}})\Big|_0^{x_0} + Akx_cw\sqrt{2\pi} + Anw\sqrt{2\pi}] \quad (12)$$

The pressure value of the channel steel at $x = x_0$ is zero, that is $kx_0 + n = 0, x_0 = -\frac{n}{k}$

Substitute $x_0 = -\frac{n}{k}$ into formula (12) to obtain the work done by the carcass homogenised distributed force on the simple supported beam as shown in formula (13):

$$W_C = \frac{b}{2s}[\sqrt{2\pi}Aw(kx_c + n) + 2Akw^2(e^{-\frac{x_c^2}{2w^2}} - e^{-\frac{(\frac{n}{k}+x_c)^2}{2w^2}}) - \frac{n^2y_0}{k}] \quad (13)$$

Summarise the data and substitute them into formulas (10) and (11). The calculated energy data are shown in the following table 1.

Since in the non-relief state, the energy absorbed by the carcass is dispersed on both sides of the load point. Now the ratio of the energy absorbed by the carcass to the total work done by the external force is defined as the energy dissipation rate of the carcass.

Part of the work done by the concentrated load on the simple supported beam acts on the air inside the inflatable carcass. The other part works on the channel steel. It can be seen from Fig.17 that as the focused load imposed on the simple supported beam increases, the proportion of the energy absorbed by the inflatable tire gas to the total energy gradually decreases. Since the simple supported beam has not entered the automatic pressure relief state, the pressure in the carcass has not reached the pressure relief threshold of the automatic pressure relief valve. As a concentrated load increases, the pressure in the carcass gradually increases. This results in a decrease in the carcass' capacity to absorb energy. This affects the inflatable carcass' homogenized force reduction effect.

5.2 Analysis and study of the unloading and load shedding effect under the state of fluid release

5.2.1 Comparative analysis of load shedding effects

The λ_2 effect is the load reduction effect of fluid released on the lining supporting structure after reaching the pressure relief threshold. When the load applied to the carcass reaches 15kN, the two different fluids of the inflatable carcass and the water-filled carcass are quantitatively relieved at *2*kPa per level. The external load remains unchanged and the external load acts on the lining structure. Based on the discharge of fluid, it shows a linear decrease trend as shown in Fig. 18.

The load reduction effect of the carcass on the supporting structure in the state of fluid discharge is produced by the combined action of the λ_1 and λ_2 effects. The change in the bending moment of the load action point with fluid discharge reflects the fluid load reduction effect, as shown in Fig. 19.

When the external load remains unchanged as the fluid leaks out, the internal pressure of the carcass continues to decrease. The force exerted by the external load on the supporting structure gradually decreases. It can be seen in Fig.19 that the bending moment at the load application point shows a linear downward trend. The bending moment reduction rates of the inflated and water-filled carcasses can be gradually increased to close to 100% from about 14% and 7% respectively.

5.2.2 Comparative analysis of pressure relief rate in fluid discharge state

It can be seen from Fig. 20 that the pressure relief rate of the inflatable carcass is about 76 Pa/s and the pressure relief rate of the water-filled carcass is about 89 Pa/s indicating that in the state of fluid discharge, water energy lowers the carcass faster than air internal pressure. The carcass under the action of external concentrated load is in high-pressure state. When fluid release reduces the internal pressure, it can also reduce the load on the simple supported beam. For the case of large deformation rates of the surrounding rock, the water-filled tire lining support structure has a better supporting effect than the inflatable tire lining support structure.

6 Conclusions and discussion

Fluid filled-lining (inflatable and water-filled matrix) is proposed to give the surrounding rock a certain amount in deformation space in response to large deformations of soft rock tunnels with high ground stresses. By

establishing the test model of the simply supported beam force of the inflatable and water-filled carcass, the force of the straight section of the tunnel support structure is simulated and the relevant tests are carried out. The following conclusions are drawn:

(1) The fluid filled lining support structure can produce fluid homogenization load reduction effect (λ_1 effect) and fluid discharge load reduction effect (λ_2 effect) in the process of supporting high in-situ soft rock tunnels.

(2) The carcass can reduce the load received within a certain range on both sides of the loaded area; the uniform load shedding effect shows a linear decreasing law with the increase of the external load; in the decompression state, the fluid discharge load shedding effect shows a linear increasing law with the fluid discharge and the decrease of the internal pressure of the carcass.

(3) Inflatable and water-filled carcasses have better homogenization force effects, but inflatable carcasss is more effective.

(4) In the no relief-pressure state, the inflatable carcass's maximum bending moment reduction rate is 28%, and the water-filled carcass's maximum is 7%. In the relief-pressure state, the inflated and water-filled carcass's maximum bending moment reduction rate can reach 100%.

(5) Calculations show that the inflatable carcass energy dissipation rate is up to 90% and varies with load. When the load increases, the energy dissipation rate decreases linearly.

(6) The test results show that the relief-pressure rate of the water-filled carcass is slightly higher than that of the pneumatic carcass, and under the same conditions, the water-filled carcass fluid discharge load shedding rate is about 1.2 times that of the pneumatic carcass.

Future work: The authors will continue to study fluid-filled lining and consider more influencing factors such as mountain water table, temperature, external forces, etc. In their future work. Mountain water is particularly influential. Mountain water has both direct and indirect effects on fluid-filled linings. The direct impact is the carcass force, resulting in uneven carcass force and unstable overall force. Also, mountain water affects surrounding rock stability, causing the rock to become unstable. The indirect influence is that groundwater will have a certain corrosion effect on the tunnel lining, reduce the bearing capacity of the surrounding rock and the tunnel lining structure, and then affect the stability of the tunnel structure, leading to collapse accidents.

Therefore, the authors will take the impact of mountain water as the next research topic, considering the force characteristics of lining structures under water pressure and the calculation method of water pressure, etc.

Declaration of Competing Interest

The authors declare that they have no known competing financial interests or personal relationships that could have appeared to influence the work reported in this paper.

Acknowledgement

This work was supported by the National Natural Science Foundation of China (No. 52079071)

Author Contributions: Formal analysis, Jie Liu and Bin Wang; carrying out experiments, Yunan Yang and Haoyu Yang; data curation, Yansong Wang and Zhuoxing Du; writing—original draft prepa-ration, Jie Liu and Bin Wang; writing—review and editing, Jie Liu , Bin Wang and Yunan Yang. All authors have read and agreed to the published version of the manuscript.

References

[1] Lei, S., Zhao, W. "Study on Mechanism of Circumferential Yielding Support for Soft Rock Tunnel with Large Deformation", Rock and Soil Mechanics, 41(3), (2020). https://doi.org/10.16285/j.rsm.2019.5545.

[2] Kanji, M. A. "Critical issues in soft rocks", *Journal of Rock Mechanics and Geotechnical Engineering* 6(3), pp.186-195 (2014). https://doi.org/10.1016/j.jrmge.2014.04.002

[3] Meng, L., Huang, Y., Li T., et al. "An improved classification method of asymmetrical squeezing large deformation of layered soft rock tunnels under high geo-stresses", *Journal of Rock Mechanics and Engineering*, 41(1), (2022). https://doi.org/10.13722/j.cnki.jrme.2021.0613

[4] Zhang, G., Deng, J., Wang, D., et al. "Mechanism and Classification of Tectonic-induced Large Deformation of Soft Rock Tunnels", *Advanced Engineering Sciences*, 53(1), (2021). https://doi.org/10.15961/j.jsuese.202000533.

[5] Guo, Q., Wu, F., Qian, W., et al. "Study on the relationship between rock deformation and in-situ stress in long-buried tunnels in Wuqiaoling", *Journal of Rock Mechanics and Engineering*,11, pp. 2194-2199 (2006). https://doi.org/10.3321/j.issn:1000-6915.2006.11.005.

[6] Chen, Z., He, C., Wu, D., et al. "Study on prediction of large deformation classification in high ground stress laminated soft rock tunnel", *Journal of Southwest Jiaotong University*, 53(6), pp. 1237-1244 (2018). http://doi.org/10.3969/j.issn.0258-2724.2018.06.020

[7] Cristescu, N., Duda, I. "A tunnel support analysis incorporating rock creep and the compressibility of a broken rock stratum", *Computers and Geotechnics*, 7(3), pp. 239-254 (1989). https://doi/org/10.1016/0266-352X(89)90051-7.

[8] Zhu, X., Yang, S., Xia, H., et al. "Joint support technology and its engineering application to deep soft rock tunnel with strong creep", *Geotechnical and Geological Engineering*,38, pp.3403-3414 (2020). https://doi.org/10.1007/s10706-020-01222-8.

[9] Li, G., Ma, F., Guo. J., et al. "Study on deformation failure mechanism and support technology of deep soft rock roadway", *Engineering Geology*, 264, (2020). https://doi.org/10.1016/j.enggeo.2019.105262.

[10] Zhao, C., Li, Y., Liu, G., et al. "Mechanism analysis and control technology of surrounding rock failure in deep soft rock roadway", *Engineering Failure Analysis*, 115, (2020). https://doi.org/10.1016/j.engfailanal.2020.104611.

[11] Srivastava, L. P., Singh, M., "Empirical estimation of strength of jointed rocks traversed by rock bolts based on experimental observation", *Engineering Geology* ,197, pp. 103-111 (2015). http://doi.org/10.1016/j.enggeo.2015.08.004.

[12] Yu, Y., Zhu C., Chong, D., et al. "Catastrophe mechanism and disaster countermeasure for soft rock roadway surrounding rock in Meihe mine", *International Journal of Mining Science and Technology*, 25(3), pp. 407-413 (2015). http://doi.org/10.1016/j.ijmst.2015.03.013.

[13] Ghorbani, M., Shahriar, K., Sharifzadeh, M., et al. "A critical review on the developments of rock support systems in high stress ground conditions", *Int.J. Min. Sci. Technol*, 30 (5), pp. 555-572 (2020). https://doi.org/10.1016/j.ijmst.2020.06.002.

[14] Wang, B., He, M., Qiao, Y., "Resistance behavior of Constant-Resistance-Large-Deformation bolt considering surrounding rock pressure", *Int. J. Rock Mech. Min.Sci*, 137, 104511 (2021). https://doi.org/10.1016/j.ijrmms.2020.104511.

[15] Arora, K., Gutierrez, M., Hedayat, A., "Physical model simulation of rock support interaction for the tunnel in squeezing ground", *J. Rock Mech. Geotech. Eng* , 14 (1), pp. 82-92 (2022). https://doi.org/10.1016/j.jrmge.2021.08.016.

[16] Ortlepp, W. D., Stacey, T. R., "Performance of tunnel support under large deformation static and dynamic loading", *Tunnelling and Underground Space Technology* ,13(1), pp. 15-21 (1998). http://doi.org/10.1016/S0886-7798(98)00022-4.

[17] Zhang, B., Zhang, Z., Wang, B., et al. "Experimental study on application of yielding bolt in large deformation tunnel support", *Geomechanics*, 37(7), pp. 2047–2055 (2016). https://doi.org/10.16285/j.rsm.2016.07.028.

[18] Yokota, Y., Zhao, Z., Nie, W., et al. "Development of a new deformation-controlled rock bolt: Numerical modelling and laboratory verification", *Tunnelling and Underground Space Technology*, 98 (2020). http://doi.org/10.1016/j.tust.2020.103305.

[19] Zhang, J., Liu, L., Liu, C., et al. "Mechanism and application of new prestressed yield bolt for controlling deep high-stress rock mass", *Tunnelling and Underground Space Technology*, 119, pp.0886-7798 (2022). https://doi.org/10.1016/j.tust.2021.104254.

[20] Fan, J., Guo, Z., Qiao, X., et al. "Constant Resistance and Yielding Support Technology for Large Deformations of Surrounding Rocks in the Minxian Tunnel", *Advances in Civil Engineering*, pp.1-13. (2020). https://doi.org/10.1155/2020/8850686.

[21] Cheng, J., Zhao, X. "Study and application of roadway support technology in high stress soft coal seam", *Coal Science and technology*, 43(5), pp. 9-12(2015). http://doi.org/10.13199/j.cnki.cst.2015.05.003.

[22] Yu, W., Wu, G., An, B. "Investigations of support failure and combined support for soft and fractured coal-rock tunnel in tectonic belt", *Geotechnical and Geological Engineering*, 36, pp. 3911-3929 (2018). http://doi.org/10.1007/s10706-018-0582-z.

[23] Barla, G,. Bonini, M., Semeraro, M. "Analysis of the behaviour of a yield-control support system in squeezing rock", *Tunnelling and Underground Space Technology*, 26(1), pp. 146-154 (2011). http://doi.org/10.1016/j.tust.2010.08.001.

[24] Wu, K., Shao, Z. "Study on the Effect of Flexible Layer on Support Structures of Tunnel Excavated in Viscoelastic Rocks", *Journal of Engineering Mechanics*, 145(10), (2019). https://doi.org/10.1061/(ASCE)EM.1943-7889.0001657.

[25] Tian, Y., Chen, W.Z., Tian, H. et al. "Parameter design of yielding layers for squeezing tunnels", *Tunnelling and Underground Space Technology*, 108, pp. 0886-7798 (2021). https://doi.org/10.1016/j.tust.2020.103694.

[26] Tian, H., Chen, W., Tan, X., et al. "Failure of rigid support and yielding support solution in large deformation tunnels: A case study", *Engineering Failure Analysis*, 140, (2022).

[27] Tian, Y., Chen, W., Tian, H., et al. "Study on design of pressure-yielding support in buffer layer considering time-dependent weakening of soft rock strength", *Geomechanics*, 41(S1), pp. 237-245 (2020). https://doi.org/10.16285/j.rsm.2019.0774.

[28] Wu, K., Shao, Z., Qin, S. "A solution for squeezing deformation control in tunnels using foamed concrete: A review", *Construction and Building Materials*, 257, (2020). http://doi.org/10.1016/j.conbuildmat.2020.119539.

[29] Wu, K., Shao, Z., Qin, S., et al. "A critical review on the performance of yielding supports in squeezing tunnels", *Tunnelling and Underground Space Technology*, 115, (2021). https://doi.org/10.1016/j.tust.2021.103815.

[30] Lei, S., Zhao, W., "Study on the mechanism of large-deformation circumferential compression support in soft rock tunnel",

Geotechnics, 41(3), pp. 1039-1047 (2020). https://doi.org/10.16285/j.rsm.2019.0545.

[31] Wu K,. Shao. Z., Sharifzadeh. M., et al. "Analytical computation of support characteristic curve for circumferential yielding lining in tunnel design", *Journal of Rock Mechanics and Geotechnical Engineering*, 14(1), pp.144-152 (2022). https://doi.org/10.1016/j.jrmge.2021.06.016.

[32] Tian, H., Tian, Y., Chen, W., et al. "Design of the yielding support used highly deformable elements for a tunnel excavated in squeezing rock", J. Mt. Sci, 20, pp. 1458–1468 (2023). https://doi.org/10.1007/s11629-022-7660-7.

[33] Zhao, W. "Structural implementation method of yielding support for deep tunnel in weak rock", *Geotechnical Engineering Technique*, 36(2), pp. 123-128 (2022). https://doi.org/10.3969/j.issn.1007-2993.2022.02.007.

[34] Dong, J., Xu, Bin., Wu, X., et al. "Elastic-plastic deformation of surrounding rocks under graded yielding support of tunnel", *Rock and Soil Mechanics*, 43(8), pp. 2123-2135 (2022). https://doi.org/10.16285/j.rsm.2021.6457.

[35] Dong, J., Xu, B., Wu, X. "Analysis of mechanical Properties of graded yielding support structure for high ground stress soft rock tunnel", *Chinese Journal of Highway*, 1-15, (2023). http://kns.cnki.net/kcms/detail/61.1313.U.20221012.1739.004.

Biographies

Jie Liu was born in Zhaotong City, Yunnan Province in 1979. He earned a master 's degree in hydraulic structure engineering from China Three Gorges University and a doctor 's degree in hydraulic structure engineering from Wuhan University in 2005 and 2008, respectively. His research interests include the theory and application of unloading rock mass mechanics and deep rock mass stability and support research. He has been published journal 101 papers.

Bin Wang was born in Kaifeng City, Henan Province in 1984. He earned a master 's degree in structural engineering from Henan University of Technology in 2009. He is currently studying for a doctorate in civil engineering from Three Gorges University. His research interests include deep rock mass stability and support research and deep foundation pit support structure research. He has published 10 journal papers.

Yunan Yang was born in Chongqing in 1979. She earned her B.S. degree from Southwest Agricultural University (now Southwest University) in 2002 and her M.S. degree from Southwest University in 2008, respectively, She is currently teaching as an associate professor in the School of Civil Engineering and Architecture at China Three Gorges University.and her main research interests are in landscape plant applications, slope ecological protection and environmental geotechnical engineering. She has published 15 papers.

Haoyu Yang was born in Shayang County, Jingmen City, Hubei Province in 1996. He earned his M.S. degree in engineering from China Three Gorges University in 2022, and he is currently working in a design institute in Guangxi Province. His research interests include in-situ stress testing of deep-buried soft rock tunnels, research on tunnel lining support technology, and research on large deformation of surrounding rocks in deep-buried soft rock tunnels with high geostress. He has published journal 1 paper.

Yansong Wang was born in Ningguo City, Xuancheng City, Anhui Province in 1998. He earned his M.S. degree in engineering from China Three Gorges University in 2023, and he is currently working at the Institute of Rural Electrification, Ministry of Water Resources. His research interests include the study of tunnel lining support technology, the study of large deformation of surrounding rock in deep-buried high geostress soft rock tunnels, and the safety monitoring of sea ponds. He has published 1 paper.

Zhuoxing Du was born in Xuecheng District, Zaozhuang City, Shandong Province in 1993. He earned his M.S. degree in engineering from Three Gorges University in 2022, and he is currently working in a private university. His research interests include the study of large deformation of surrounding rocks in high geostress layered schist tunnels, and the study of impact resistance and seismic isolation performance of tunnel linings. He has published one paper and has been authorized three invention patents.

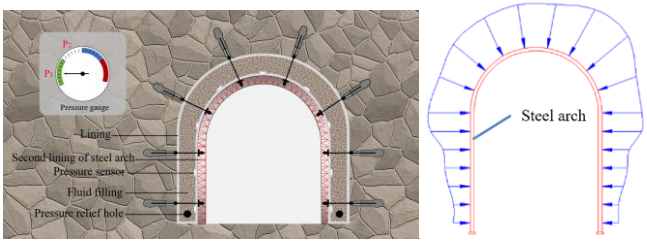

a) The initial installation stage of fluid-filled lining and the force diagram of its supporting structure

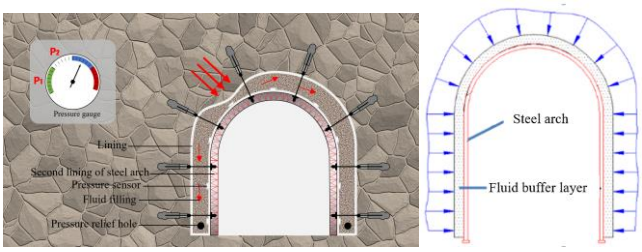

b) The pressure diagram of the homogenisation pressurization stage and its supporting structure below the pressure relief threshold

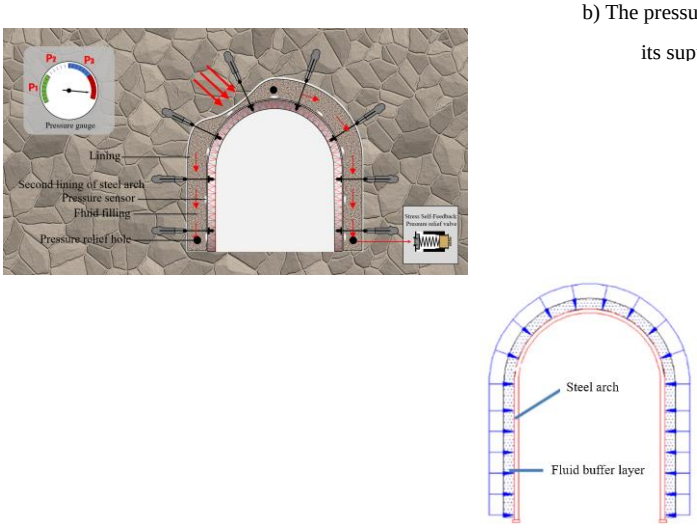

c) The automatic pressure relief stage of fluid filled lining and the force diagram of its supporting structure

Fig.1 Schematic diagram of the three-stage principle

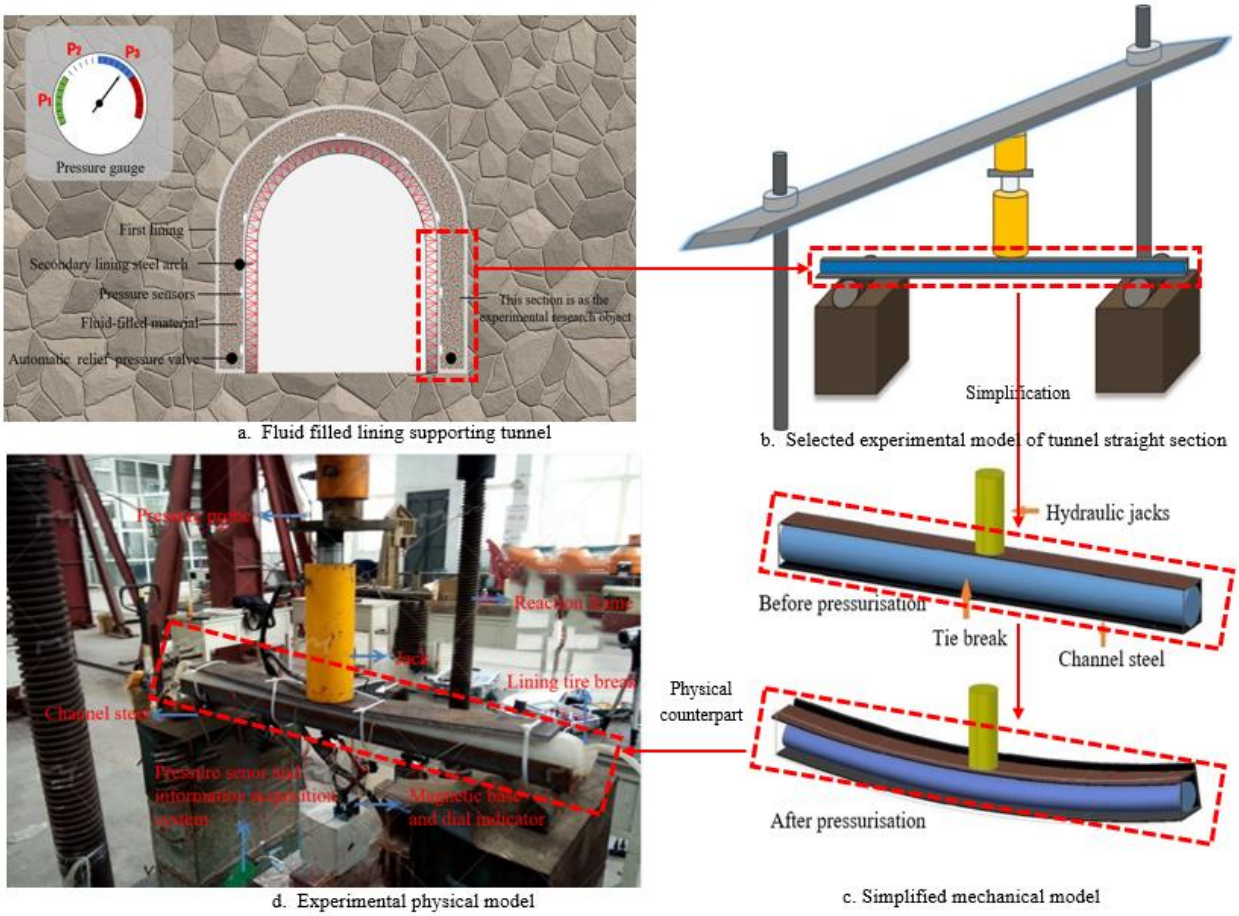

Fig.2 Test of simple supported beam of carcass lining

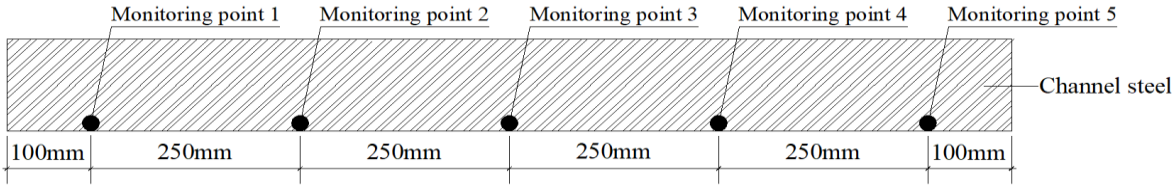

Fig.3 Layout of monitoring points

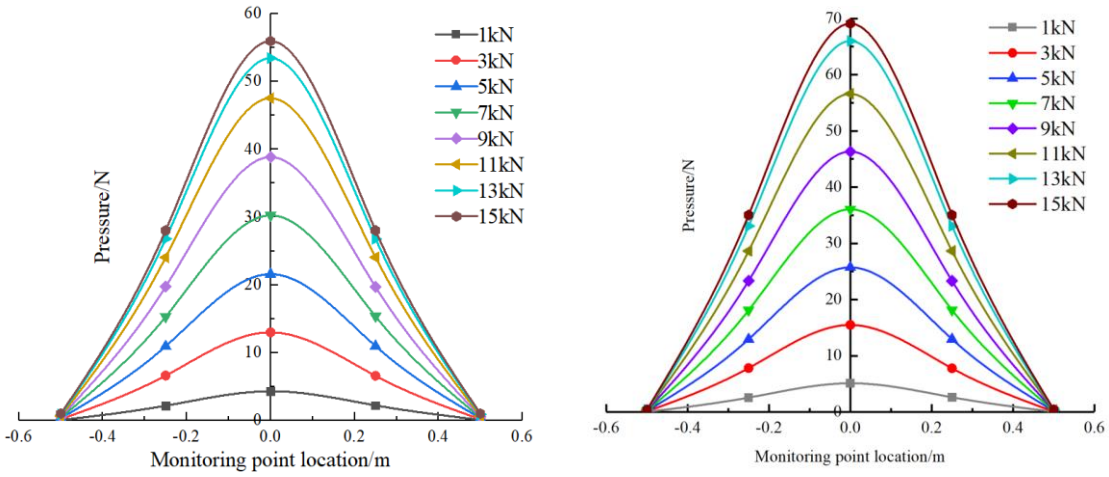

Fig. 4 Pressure distribution diagram under different load levels

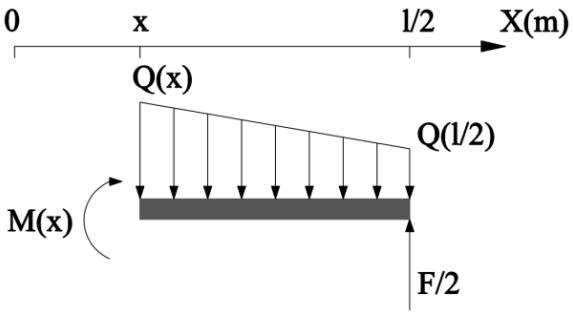

Fig.5 Force analysis diagram of the right section of a simple supported beam

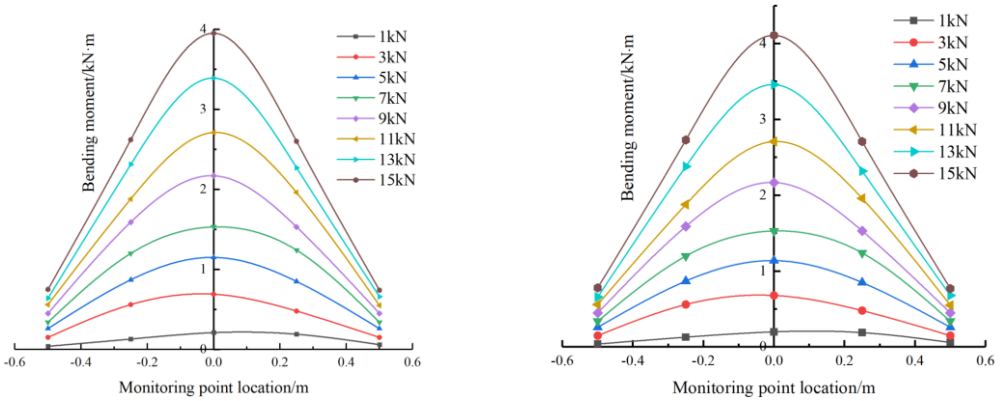

a. Bending moment distribution of inflatable carcass

b. Bending moment distribution of water-filled carcass

Fig.6 Bending moment distribution diagram under different load levels

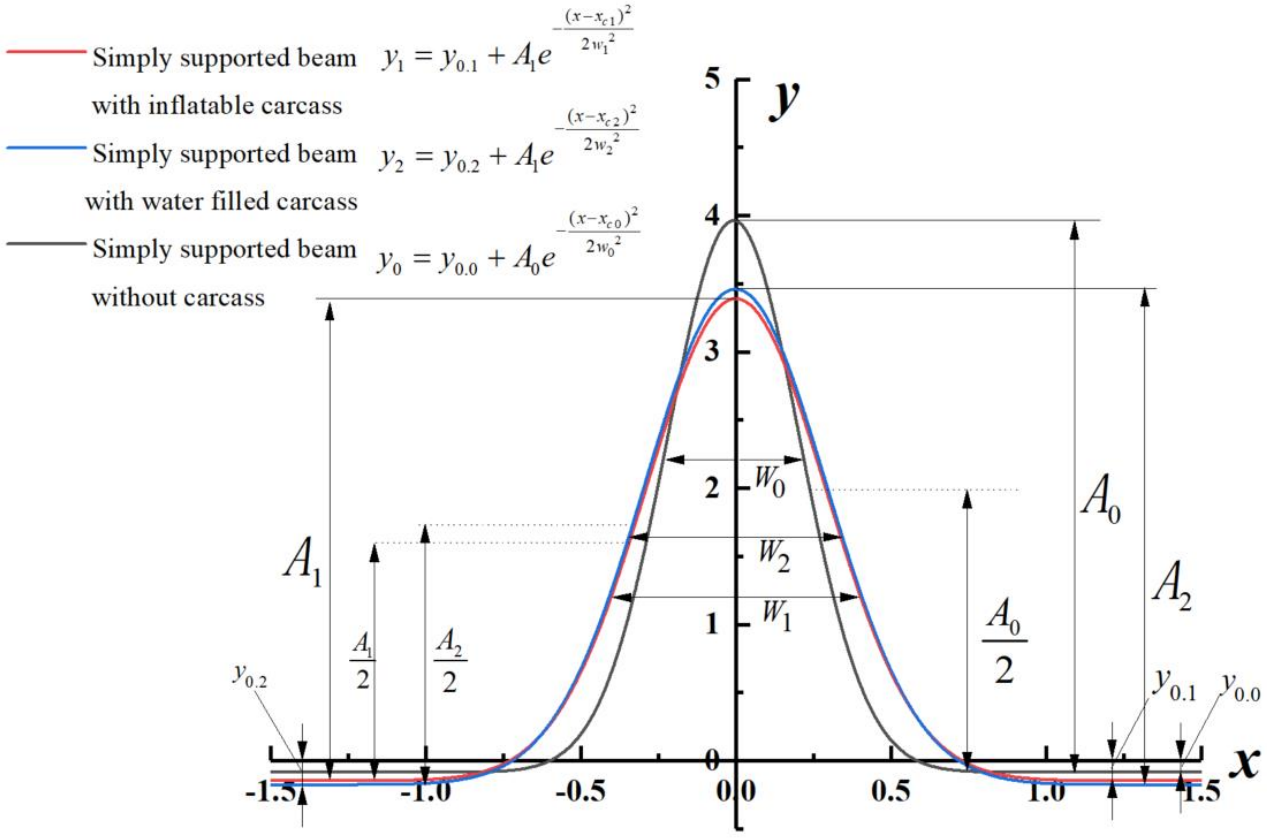

Fig.7 Analytical diagram of bending moment distribution formula

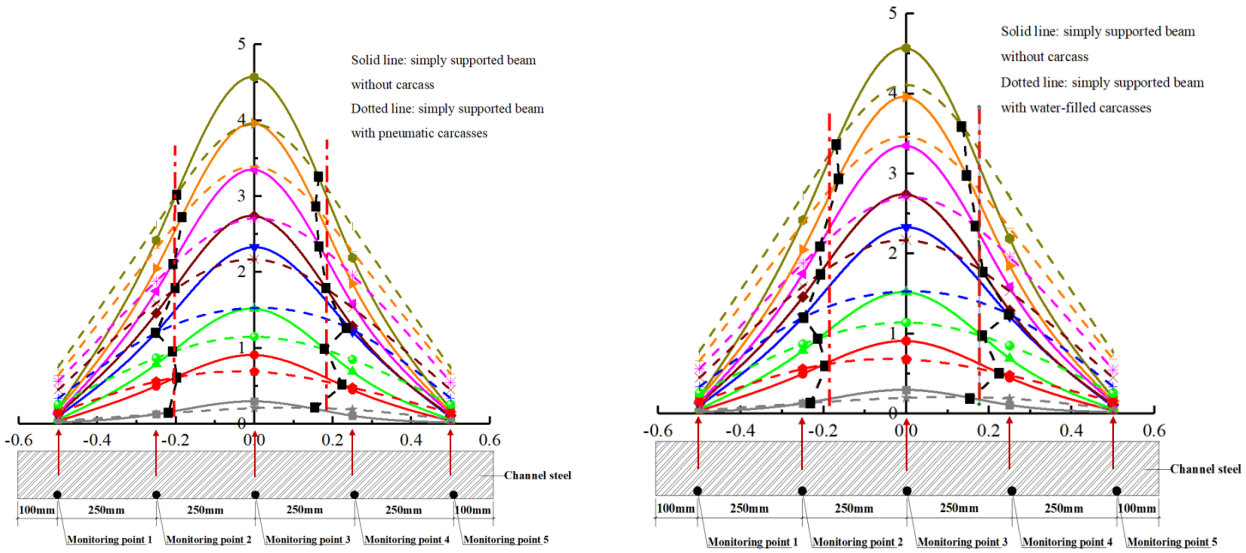

a. Distribution of bending moment reduction ranges for pneumatic carcasses

b. Distribution of bending moment reduction ranges for water-filled carcasses

Fig.8 Distribution of bending moment reduction range under different load vels

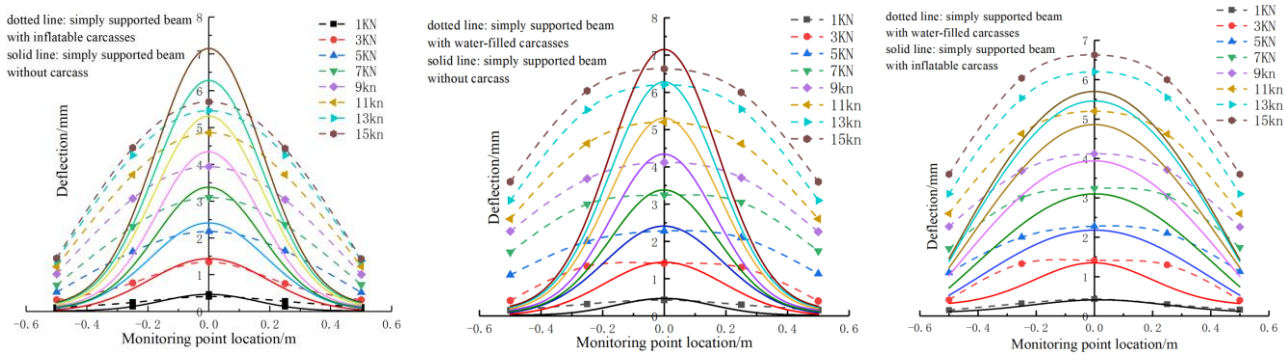

a. Deflection comparison of inflatable carcass and without carcass

b. Deflection comparison of water-filled carcass and without carcass

c. Deflection comparison of inflatable carcass and water-filled carcass

Fig. 9 Deflection comparison diagram

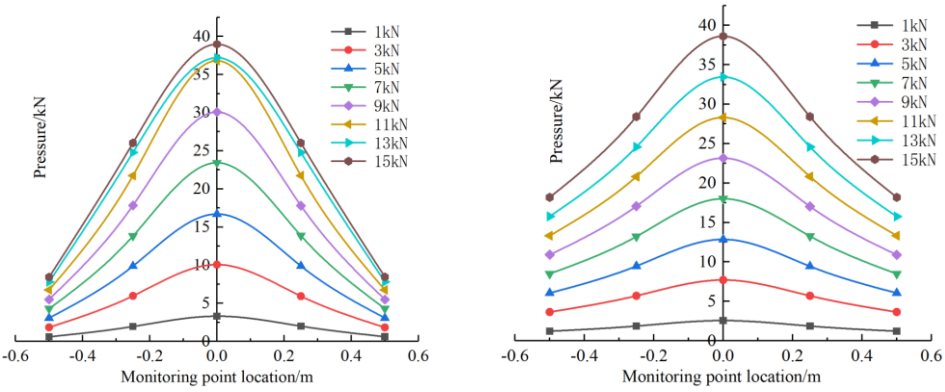

a. Pressure distribution of inflatable carcasses under different levels of loading at a loading rate of 0.05kN/s

b. Pressure distribution of inflatable carcasses under different levels of loading at a loading rate of 0.02kN/s

Fig. 10 Pressure distribution of inflatable carcasses under different loading rates and load ratings

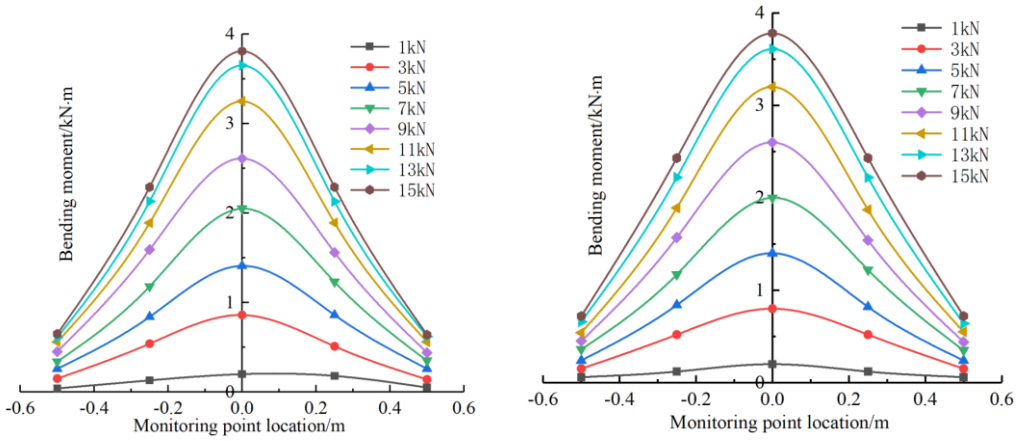

a. Bending moment distribution of inflatable carcasses under different levels of loading at a loading rate of 0.05kN/s

b. Bending moment distribution of inflatable carcasses under different levels of loading at a loading rate of 0.05kN/s

Fig. 11 Bending moments distributionof inflatable liner carcasses under different loading rates and load ratings

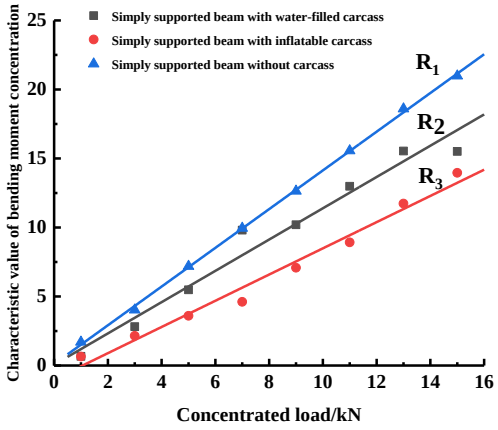

Fig.12 Characteristic values of bending moment distribution concentration under different load levels

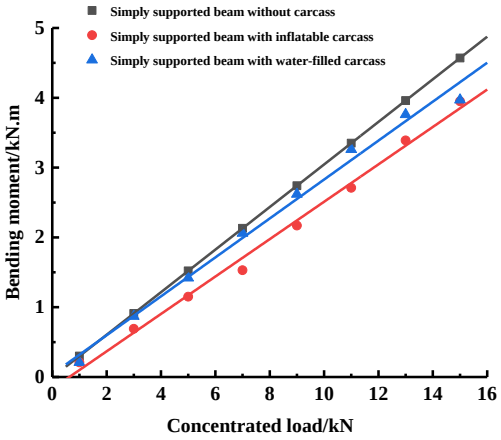

Fig.13 Comparison diagram of mid-span bending moment of simple supported beam

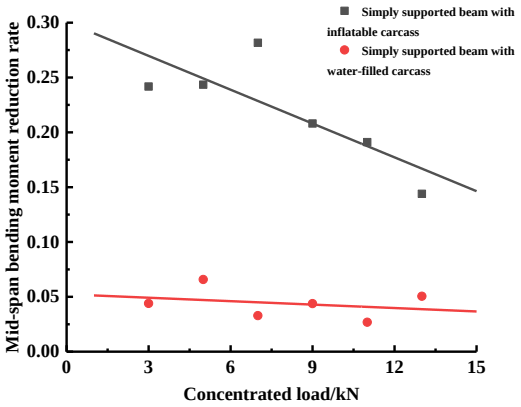

Fig.14 Analysis diagram of bending moment reduction rate in mid-span

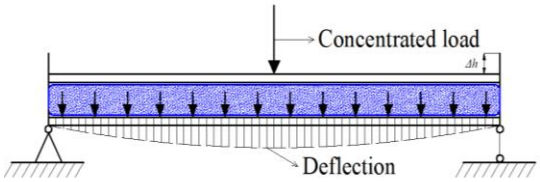

Fig.15. Force model of simple supported beam of carcass

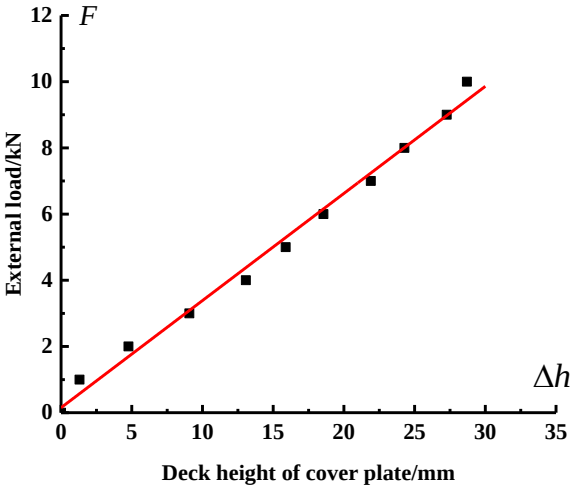

Fig. 16 The relationship between the external force of loading and the falling height of the cover plate

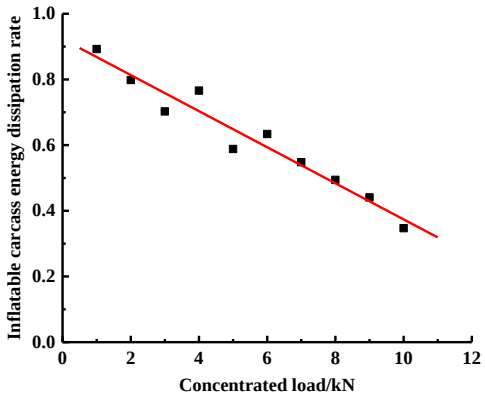

Fig.17 The energy dissipation rate of the carcass changes with the load

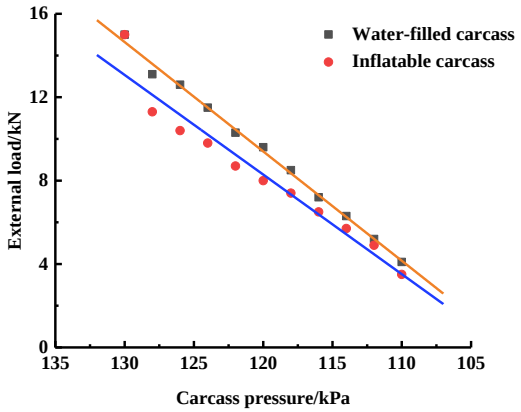

Fig.18 The load acting on the lining structure changes with the carcass pressure

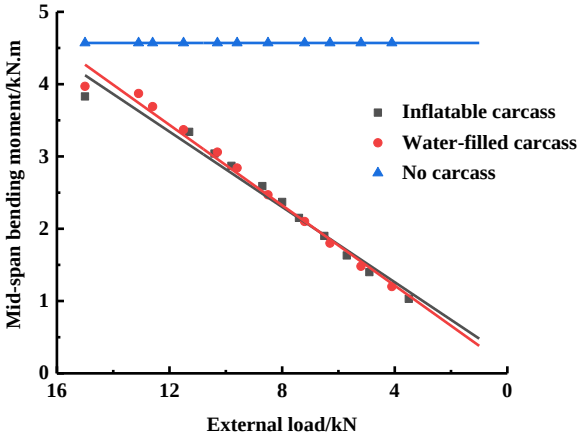

Fig.19 Bending moment change law in the state of fluid release

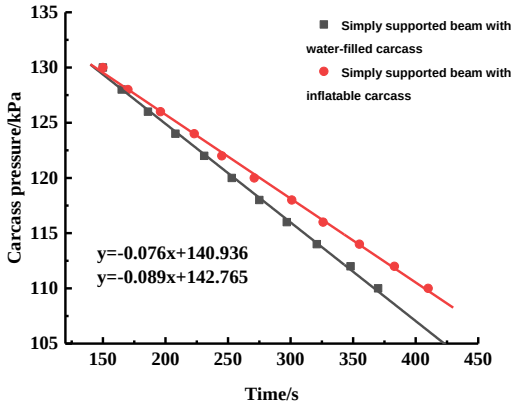

Fig.20 Comparison of carcass pressure relief rate

Table 1 The energy received by the channel steel with different concentrated forces when the simple supported beam does not reach the automatic pressure relief state

External force	1 kN	2 kN	3 kN	4 kN	5 kN	6 kN	7 kN	8 kN	9 kN	10 kN
WC/J	0.07	0.48	1.35	1.53	3.27	3.40	4.95	6.14	7.63	9.37
WT/J	0.58	1.90	3.19	5.01	4.67	5.88	6.00	6.00	6.01	4.98
W/J	0.65	2.38	4.54	6.54	7.94	9.28	10.95	12.14	13.64	14.35